Integrated charge and seal assessment in the Monagas fold and thrust belt of Venezuela

Martin Neumaier, Ralf Littke, Thomas Hantschel, Laurent Maerten, Jean-Pierre Joonnekindt, and Peter Kukla

ABSTRACT

Conventional basin and petroleum systems modeling uses the vertical backstripping approach to describe the structural evolution of a basin. In structurally complex regions, this is not sufficient. If lateral rock movement and faulting are inputs, the basin and petroleum systems modeling should be performed using structurally restored models. This requires a specific methodology to simulate rock stress, pore pressure, and compaction, followed by the modeling of the thermal history and the petroleum systems. We demonstrate the strength of this approach in a case study from the Monagas fold and thrust belt (Eastern Venezuela Basin). The different petroleum systems have been evaluated through geologic time within a pressure and temperature framework. Particular emphasis has been given to investigating structural dependencies of the petroleum systems such as the relationship between thrusting and hydrocarbon generation, dynamic structure-related migration pathways, and the general impact of deformation. We also focus on seal integrity through geologic time by using two independent methods: forward rock stress simulation and fault activity analysis. We describe the uncertainty that is introduced by replacing backstripped paleogeometry with structural restoration, and discuss decompaction adequacy. We have built two end-member scenarios using structural restoration, one assuming hydrostatic decompaction, and one neglecting it. We have quantified the impact through geologic time of both scenarios by analyzing important parameters such as rock matrix mass balance, source rock burial depth, temperature, and transformation ratio.

Manuscript received September 12, 2012; provisional acceptance February 02, 2013; revised manuscript received October 01, 2013; final acceptance January 13, 2013.
DOI: 10.1306/01131412157

AUTHORS

MARTIN NEUMAIER ~ *Institute of Geology and Geochemistry of Petroleum and Coal, Energy and Mineral Resources (EMR), RWTH Aachen University, Lochnerstr. 4-20, 52056 Aachen, Germany; Schlumberger, Ritterstr. 23, 52072 Aachen, Germany; mneumaier@slb.com*

Martin Neumaier received his master's degree in geological reservoirs at the University of Montpellier (France) in 2008. He joined Schlumberger in 2008 as a geologist and is currently preparing a Ph.D. at RWTH Aachen University. Martin's background and research interests are centered on geodynamics and basin evolution, regional and structural geology, petroleum systems modeling and analysis, hydrocarbon exploration, and play to prospect resource evaluation.

RALF LITTKE ~ *Institute of Geology and Geochemistry of Petroleum and Coal, Energy and Mineral Resources (EMR), RWTH Aachen University, Lochnerstr. 4-20, 52056 Aachen, Germany; ralf.littke@emr.rwth-aachen.de*

Ralf Littke received his diploma in geology and Ph.D. at Ruhr-University Bochum (Germany). He is professor of geology and geochemistry of petroleum and coal and currently dean of the faculty of Georesources and Material Science at RWTH Aachen University. His research interests include sedimentary basin dynamics, petroleum and source rock geochemistry, porosity and permeability of low-permeability rocks, natural gas geochemistry, organic petrology, petroleum system modeling, and petroleum geology.

THOMAS HANTSCHEL ~ *Schlumberger, Ritterstr. 23, 52072 Aachen, Germany; thantschel@slb.com*

Thomas Hantschel received his Ph.D. in numerical modeling in 1987 and worked for IES (Integrated Exploration Systems) as the main developer of the numerical simulator of the PetroMod (Mark of Schlumberger) Basin and Petroleum Systems Modeling software. In 2002, he became the managing director of IES, which was acquired by

Schlumberger in 2008. Thomas' research interests are centered on heat flow, pore pressure and fluid flow, rock stress, geochemical models, unconventional petroleum systems, domains in which he has contributed many publications. He is currently center manager of the Aachen-based Technology Center for Petroleum Systems Modeling and Exploration Geology.

LAURENT MAERTEN ~ *Schlumberger, 340 rue Louis Pasteur, Grabels, France; lmaerten@slb.com*

Laurent Maerten received his Ph.D. in geology and environmental sciences in 1999 from Stanford University (USA) in collaboration with Norsk Hydro. He worked at the French Petroleum Institute in Paris (France) as a research engineer in structural geology for two years. In 2004, Laurent founded the structural geology company IGEOSS, of which he was the CEO and principal consultant. He joined Schlumberger in 2010 with its acquisition of IGEOSS. His main interests are structural geology and geomechanics with a strong focus on rock and fracture mechanics, structural restoration, and applications to unconventional reservoirs.

JEAN-PIERRE JOONNEKINDT ~ *Schlumberger, 340 rue Louis Pasteur, Grabels, France; jjoonnekindt@slb.com*

Jean-Pierre Joonnekindt received his master's degree in structural geology in 1994 from the Earth Sciences Montpellier University (France), in collaboration with Jean-Pierre Petit, and a master's degree in computer sciences in 2000 from the Joseph Fourier Grenoble University (France). He joined IGEOSS in 2008 as a structural geology consultant, and Schlumberger in 2010 with its acquisition of IGEOSS. His interests focus on geological structures, 2D and 3D restoration, geomechanics, fracture mechanics, and the development of innovative methods to improve hydrocarbon production in fractured reservoirs.

PETER KUKLA ~ *Geological Institute, Energy and Mineral Resources (EMR), RWTH Aachen University, Wuellnerstr. 2, 52062 Aachen, Germany; kukla@geol.rwth-aachen.de*

INTRODUCTION

Basin and petroleum systems modeling (BPSM) is essential to petroleum exploration because it provides quantitative estimates of the hydrocarbon charge history (hydrocarbon generation, migration, accumulation, and respective timing) and enables hydrocarbon volume and property predictions (Hantschel and Kauerauf, 2009). Basin and petroleum systems modeling is also commonly used for pore pressure prediction as an alternative to seismic velocity–derived pore pressure prediction, especially where the seismic data quality is poor; for example, in subsalt and subthrust settings. Standard BPSM is, however, limited for complex basin geometries, especially in areas with thrusting and salt movement. In these areas, structural restoration, which accounts for lateral rock movement caused by faulting and folding, should be applied to describe the geometrical evolution of a basin. Recently, structural restoration methods incorporate geomechanics during the restoration process while keeping a record of the evolving strain and stress distributions (Maerten and Maerten, 2006). The structurally restored paleogeometries (structural geometry of the basin at a given geologic time) can then be used in BPSM, replacing the conventional backstripping method. The integration of structural restoration into BPSM provides a better understanding of the petroleum system's evolution through geologic time in complex tectonic settings. This workflow has been successfully applied to several case studies with both two-dimensional (2D) and three-dimensional (3D) models (e.g., Baur et al., 2009).

The traditional stress–strain model has also undergone recent improvements. To more accurately predict a compaction-related decrease in porosity, lateral compressional boundary conditions can be applied, resulting in higher horizontal stresses and pore pressures (Hantschel et al., 2012). This advanced method replaces the simple approach using vertical lithostatic pressure (Terzaghi, 1923), which is simply equal to overburden load. The evolution of geomechanical properties calculated by a combined approach of structural restoration and BPSM analysis can assist in predicting fracturing and/or seal integrity through geologic time.

In this paper, we describe the theoretical background of the concept as well as its applicability and limitations. Dynel software for structural restoration and PetroMod (Mark of Schlumberger) software for petroleum system modeling were applied in a combined 2D basin and petroleum systems analysis workflow of the western Monagas fold and thrust belt (Venezuela). This workflow enabled us to describe the compaction, pressure, and temperature history, and evolution of the different petroleum systems through geologic time. Structural controls on the petroleum systems, such

as the effects of thrusting on pressure and hydrocarbon generation, dynamic structure-related migration pathways, and the general impact of deformation are described. Additionally, we evaluated seal integrity by analyzing simulated stresses through geologic time.

GEOLOGIC SETTING

The Eastern Venezuela Basin (Figure 1A) is bounded by the Serrania del Interior and the El Pilar fault to the north, by a dextral strike-slip fault system at the interface of the Caribbean and South American tectonic plates, and by the Orinoco River and the Precambrian Guyana shield to the south (Hedberg, 1950; Passalacqua et al., 1995; Pindell and Tabbutt, 1995). The northern parts of the basin, the Monagas fold and thrust belt, override a less deformed foreland part of the basin to the south.

The basin initially formed as a passive margin on the South American shield following late Jurassic to early Cretaceous rifting. During the transcollision of the Caribbean plate with the South American plate in the late Cenozoic, subsidence became flexural, and extensive folding and thrusting occurred in the northern part of the basin (Figure 1B). Roure et al. (2003) described both the geodynamic history and the stratigraphy (Figure 1C). Cenozoic platformal and basinal facies of the passive margin overlie the Mesozoic sediments, which include the prerift and synrift sequences. The most recent sediments belong to the synorogenic north-sourced depositional sequence. The principal source rocks in the area are within the Querecual and San Antonio Formations of the Guayuta Group (Talukdar et al., 1988; Gallango et al., 1992; Alberdi and Lafargue, 1993). These mudstones are characterized by type II kerogen with 2 to 6 wt% total organic carbon (TOC) for partly highly mature samples. Hydrogen index (HI) values are as high as 500 mg HC/g TOC. Summa et al. (2003) suggested an initial TOC as high as 12% for present-day values of up to 8%, with an HI as high as 700 mg HC/g TOC. Minor source rocks exist in the Carapita Formation, particularly in the basal part, with mixed type III/II kerogen; Summa et al. (2003) estimated TOC up to 4.5% and an HI of 350 mg HC/g TOC. They also discussed the presence of Jurassic and Albian source rocks in the Serrania del Interior.

Surface oil seeps and asphalt lakes are very common in this area, and hydrocarbons have been found since the early 20th century (Young, 1978; Carnevali, 1988; Krause and James, 1989; Aymard et al., 1990; James, 1990, 2000a, 2000b; Erlich and Barrett, 1992; Prieto and Valdes, 1992). In the south, heavy oil and tar sands (Oronico Oil Belt; see Figure 1A) and conventional oil accumulations are abundant. In the thrust area, the Furrial trend

Peter Kukla is a professor of geology and director of the Geological Institute at RWTH Aachen University since 2000. He worked for Shell International in the Netherlands (1991–1996) and in Australia (seconded to Woodside Energy in Perth, 1996–2000). Peter graduated with degrees in geology from Wuerzburg University, Germany (M.Sc., 1986) and Witwatersrand University, South Africa (Ph.D., 1991). His research interests include basin analysis, clastic and carbonate reservoir characterization, unconventional gas, geodynamics of salt basins, and pore pressures.

ACKNOWLEDGMENTS

We thank Francois Roure (Institut Francais du Petrole), Sandro Serra (Serra GeoConsulting), and an anonymous reviewer for their comments and suggestions. Ian Bryant, Martin Rohde, Adrian Kleine, Alan Monahan, Will Stapley, Armin Kauerauf, and Thomas Fuchs (Schlumberger) also provided very helpful technical contribution, discussions, and internal reviews.

The AAPG Editor thanks the following reviewers for their work on this paper: Francois M. Roure, Sandro Serra, Carl K. Steffensen, and an anonymous reviewer for their work on this paper.

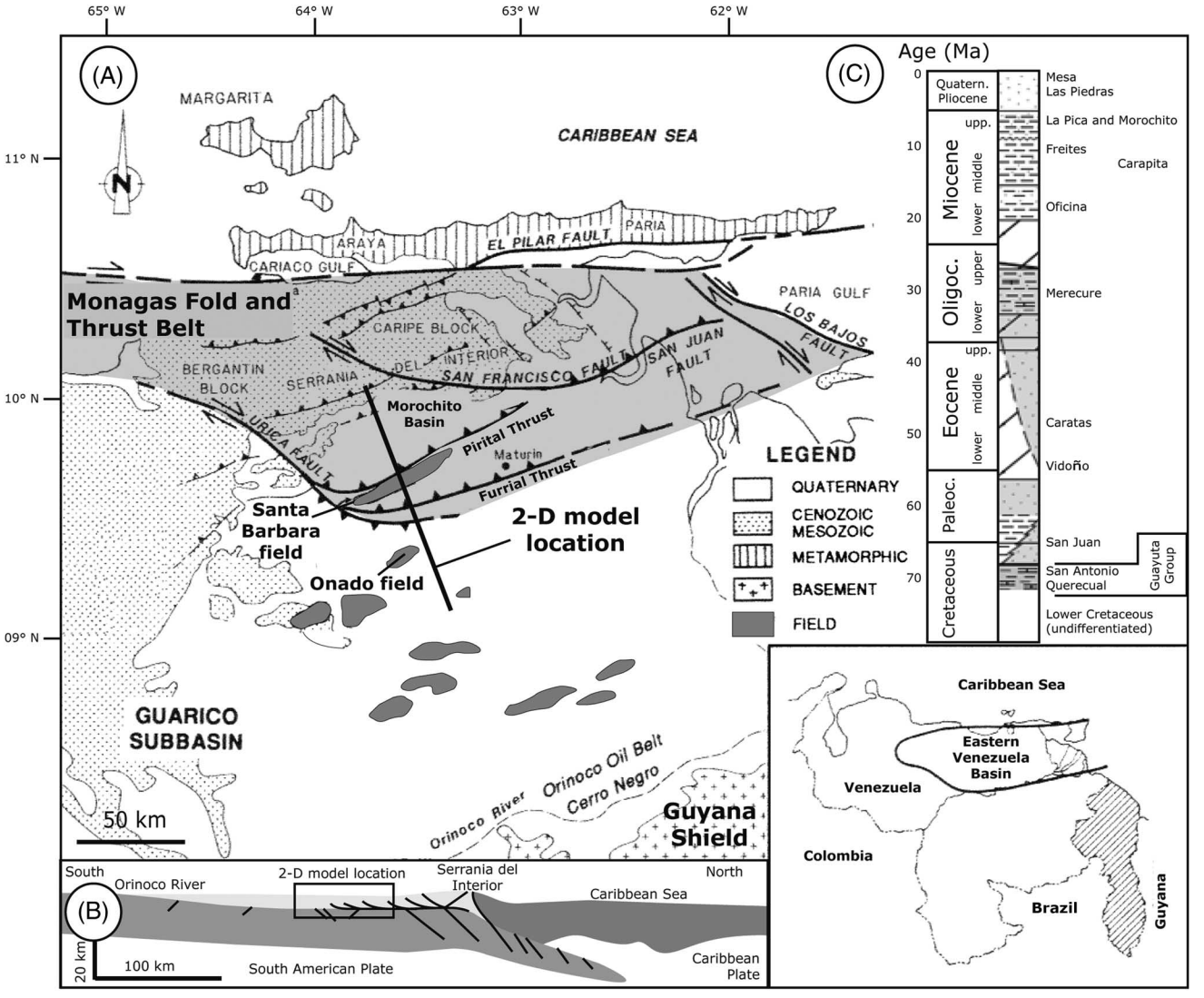

Figure 1. (A) Map of the Eastern Venezuela Basin showing structural elements and hydrocarbon occurrence (modified after Parnaud et al., 1995). Solid line shows location of two-dimensional (2D) line modeled in this study. (B) Generalized north–south geodynamic cross section of the study area (modified after Chevalier, 1987). (C) Synthetic stratigraphy of the southern foreland basin of the Eastern Venezuela Basin (modified after Roure et al., 2003).

contains some of the world's largest oil reserves for basins with this type of tectonics. Many shallow oil fields in the Eastern Venezuela Basin are located in Neogene sandstone reservoir rocks (Las Piedras, La Pica, Morichito, Chapapotal, Freites, and Oficina fields). Other reservoir formations are the synorogenic Miocene Naricual Formation and the Oligocene Merecure Formation, which are part of a proximal passive-margin sequence that shales out toward the north. The latter is the main reservoir in the thrusted Furrial trend. In the deeper passive-margin sequence, there are potential reservoirs in the Mesozoic (e.g., San Juan Formation). Because of its shaly lithology, large thickness, and lateral continuity, the synorogenic Carapita Formation is probably the most effective seal. However, several other formations have good sealing capacities, even though not well compacted, as numerous fields at shallow depths prove.

The first publications on the thermal history of the Eastern Venezuela Basin were based on one-dimensional (1D) models. Because of the complexities leading to multiple sequences caused by overthrusting, modeling was done either in the unthrusted area or, if within the thrusted area, only for geologic time intervals preceding thrusting

(Talukdar et al., 1988). Summa et al. (2003) published multiple 1D models over a large area and extrapolated the results onto regional maturity maps for the Guayuta Group and Cenozoic source rocks. These maps include a hanging-wall cutoff and therefore do not represent the higher maturities found in the thrust wedges. Elsewhere, the authors suggested that most source rocks have been in the oil window in the past. A present-day drainage area analysis of the top Cretaceous structure map was used to describe the southward charge from the deeper kitchen into the foreland basin. This regional migration model explains oil provenance and quality. Important timing aspects, such as the relationship between the structural history and source rock maturation and expulsion, are described using a regional structural restoration in conjunction with the 1D models. Parra et al. (2011) included the thrusting effect by using a 1.5D module, mimicking lateral rock transportation that is due to thrusting. Gallango and Parnaud (1995) performed 2D modeling, including hydrocarbon migration, in the unthrusted southern area. They also described a second model within the thrusted area that simulates the basin history prior to compression (from the Mesozoic to early Miocene). This model proposes long-distance petroleum migration southward before the transpressional event, which resulted in the observed structural complexity. In other papers, Roure et al. (2003), Schneider (2003), and Schneider et al. (2004) described fluid flow, pore fluid history, and diagenetic processes in a 2D model along a cross section parallel to the location of the model presented here.

MODELING METHODS

To address the charge and seal history of the Santa Barbara transect (Figure 1) in the western Monagas fold and thrust belt, we applied a combined approach using BPSM and structural restoration. A BPSM is a dynamic model of the subbasin's physical processes, such as pore pressure and temperature evolution and the development of the petroleum systems including hydrocarbon generation, expulsion, migration, accumulation, and preservation (Hantschel and Kauerauf, 2009). The BPSM is performed in 1D (on a well or pseudowell), in 2D (usually along a seismic section), and in 3D. The BPSM can also provide predictions about seal capacity and integrity, especially if field data are available for calibration.

In contrast to a static model, which consists only of geometry and properties for present day (as observed), a dynamic earth model includes the evolution of geometry and properties. The paleogeometry—or structural geometry of the model at a given geologic age (or simulation time step)—is strongly dependent on the paleowater depth (geometrical boundary condition), faulting activity, the lithology of the various layers, and their associated compaction behavior. Approaching accurate paleogeometry is crucial for achieving consistent results, especially for fluid flow simulations. In standard BPSM, the paleogeometries are automatically generated using a simplified restoration approach known as backstripping (Figure 2A, B).

Geomechanically based structural restoration uses the present-day interpreted and depth-converted geometry of a sedimentary basin or subbasin for the restoration of the basin structure backward in geologic time (Figure 2C, D). This is done by sequentially removing the syntectonic sedimentary layers from the youngest to the oldest (the reverse of deposition), allowing unfolding and unfaulting during the restoration (the reverse of deformation). In contrast to the simple backstripping approach, structural restoration allows much more control through additional geometrical boundary conditions such as lateral movement of rocks along faults or bedding slip. Recent development has resulted in geomechanical restoration algorithms, extending the pure geometrical approach by applying physical laws of rock deformation (Maerten and Maerten, 2006). The paleogeometries obtained by structural restoration are then used to describe basin geometry through time in a petroleum systems model.

The backstripping approach is applied to tectonically undisturbed areas and to areas where faulting occurred much earlier than the main phase of hydrocarbon generation (typically a sag basin or the postrift sequence of a passive margin; Figure 2A). In basins where extensional faulting occurred and where fault slip has an important horizontal component (e.g., listric faults), backstripped paleogeometries show "spiky" artifacts (Figure 2B); these paleogeometries

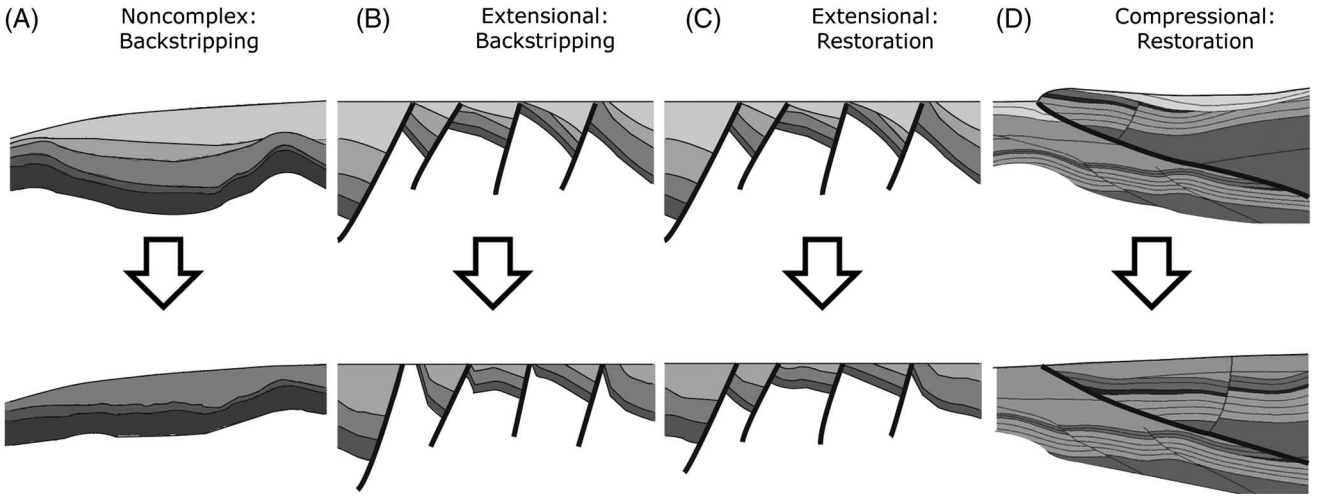

Figure 2. Steps for (A, B) backstripping and (C, D) structural restoration of geometries of different structural complexity. For details, see text.

are generally not good enough for predicting prefaulting hydrocarbon migration, but might be acceptable for hydrocarbon generation modeling. Here, structurally restored paleogeometries are important for the layer shape in the proximity of faults, and when cross-fault connectivity (like sand–sand overlaps) matters (Figure 2C). Alternatively, manual correction of paleothickness can be done. In halokinetic settings, backstripping is generally superimposed by simple salt reconstruction workflows (area balancing and extrapolation). Structural restoration should also be considered if salt movement results in geometries that are more complex. In any case, thermal modeling in the vicinity of salt is difficult due to its extremely high thermal conductivity. In areas with overthrusting or overturned folds (Figure 2D) with multiple stratigraphic sequences, typically a fold and thrust belt, backstripping fails completely because lateral rock movements are missing. In the latter case, paleogeometries need to be generated by means other than backstripping (from simple conceptual drawing to true structural restoration).

Paleogeometries generated from structural restorations can be loaded into BPSM software as an alternative to performing a calculation from backstripping. Meshing is done section per section (time step per time step), and tracking of cells from one section to the other is following rules described in Hantschel and Kauerauf (2009). For the ages corresponding to the paleosection, the basin geometry is fixed; it is not a function of compaction-controlled forward modeling as is the case when using backstripping. The BPSM simulation is restricted to the calculation of properties such as porosity, overpressure, temperature, vitrinite reflectance (R_o), and source rock maturity, which populate the fixed paleogeometries, as well as hydrocarbon migration. These compaction-controlled results are not used to adjust the depositional amounts and to correct the paleogeometry as done in the backstripping approach, and consequently geometry optimization cannot be performed. The possible difference between the compaction-law-controlled porosity change and the predefined geometry change is indirectly compensated by the corresponding adjustment of the solid grain mass.

When paleogeometries are used for basin analysis and BPSM, some factors become very important. Restoration must focus toward a best estimate paleowater depth, because changes in slope directions and topography can largely affect fluid flow. Erosion should be estimated and reconstructed, and many geologic events need to be taken into account to increase the resolution through time for dynamic modeling. The sediment thickness must be corrected in geologic time for decompaction. All these factors, which are common sources of uncertainty, are critical for a geologically meaningful restoration.

Because of the optimization method just described, adequately decompacted paleogeometries

are required from structural restoration. Inadequate decompaction can produce large errors, resulting in an unbalanced mass of solid rock matrix, underestimated source rock paleoburial depth, and deviated paleomigration paths related to differential compaction. However, it is difficult to define adequate decompaction. As a rule of thumb, in normally pressured clastic basins where the main compaction driver is linearly increasing effective stress, simple hydrostatic decompaction laws, such as those described by Athy (1930), can be used for restoration. In cases of abnormal pressure (overpressure), hydrostatic decompaction overestimates the effective stress, or underestimates porosity, and might fail to the same degree as restoration neglecting decompaction. One might be scaling normal decompaction curves wherever regional overpressure occurs and has occurred. In basins with complex erosion, pressure, and diagenetic histories, optimization loops (using BPSM simulated properties for optimized decompaction in second restoration) might be necessary. Any sort of decompaction in a carbonate-dominated environment, where compaction is generally less understood because of the effect of mineral transformations and cementation, is subject to much larger uncertainty. The question of whether to use hydrostatically decompacted or nondecompacted structurally restored paleogeometries is discussed in the section on uncertainty analysis.

MODELING

Prior to structural restoration, we performed several 1D simulations. These generated erosion and paleoaltitude estimations for structural restoration and provided a calibration for the 2D model. One-dimensional modeling also gave the first information on hydrocarbon generation and timing to identify the period of first source rock maturation ("critical moment" as defined by Magoon and Dow, 1994). This is very important because prior to structural restoration, its identification indicates when additional time steps are needed to increase time resolution for critical time intervals so that the active petroleum system can be dynamically modeled in an adequate way. However, for simulation, regular time steps are needed not only during the critical moment, but also for the entire basin history.

Structural Restoration

The following section describes our structural restoration results, shown in Figure 3, of the post-rift structural evolution of the Monagas fold and thrust belt. It can be divided into three main steps. (1) From the Mesozoic to Oligocene, the Monagas area formed parts of the northern passive margin of the South American shield (Figure 3A). The subsidence driver was mostly thermal cooling and isostatic load, with only a few normal faults. The sediments were sourced by the craton in the south. (2) In the early Miocene, the margin experienced compression from the transcollision with the Caribbean plate (Figure 3B). Two major normal faults that formed during rifting were inverted in the course of the collision, generating the regional Furrial and Pirital thrusts. Synorogenic deposits were covered by the thrusted allochthon, and intramontane piggyback basins were formed. With increasing uplift and erosion (middle Miocene, Figure 3C), their sediment fills were redeposited to form the important syntectonic Oficina and Carapita Formations south of the thrusts. (3) From late Miocene on, the late compressional phase started. Figure 3D shows the present-day structure of the Monagas fold and thrust belt (2D model crossing the Santa Barbara field). According to our restoration, the total shortening on the section, accommodated by the thrusts during the compression, is around 40 km (24.86 mi), which corresponds to 35%. It is important to note that the Pirital thrust was active until late Miocene, as indicated by the fault displacement analysis (Figure 4). These late tectonic movements might have an important effect on the seal integrity of prospects that are in the vicinity of the thrust.

Model Input Data

Table 1 shows geologic ages, lithologies, and petrophysical parameters that were assigned to our 2D model. For the main source rocks (Querecual and San Antonio Formations), a type II B kinetic was assigned (Pepper and Corvi, 1995). As a base case,

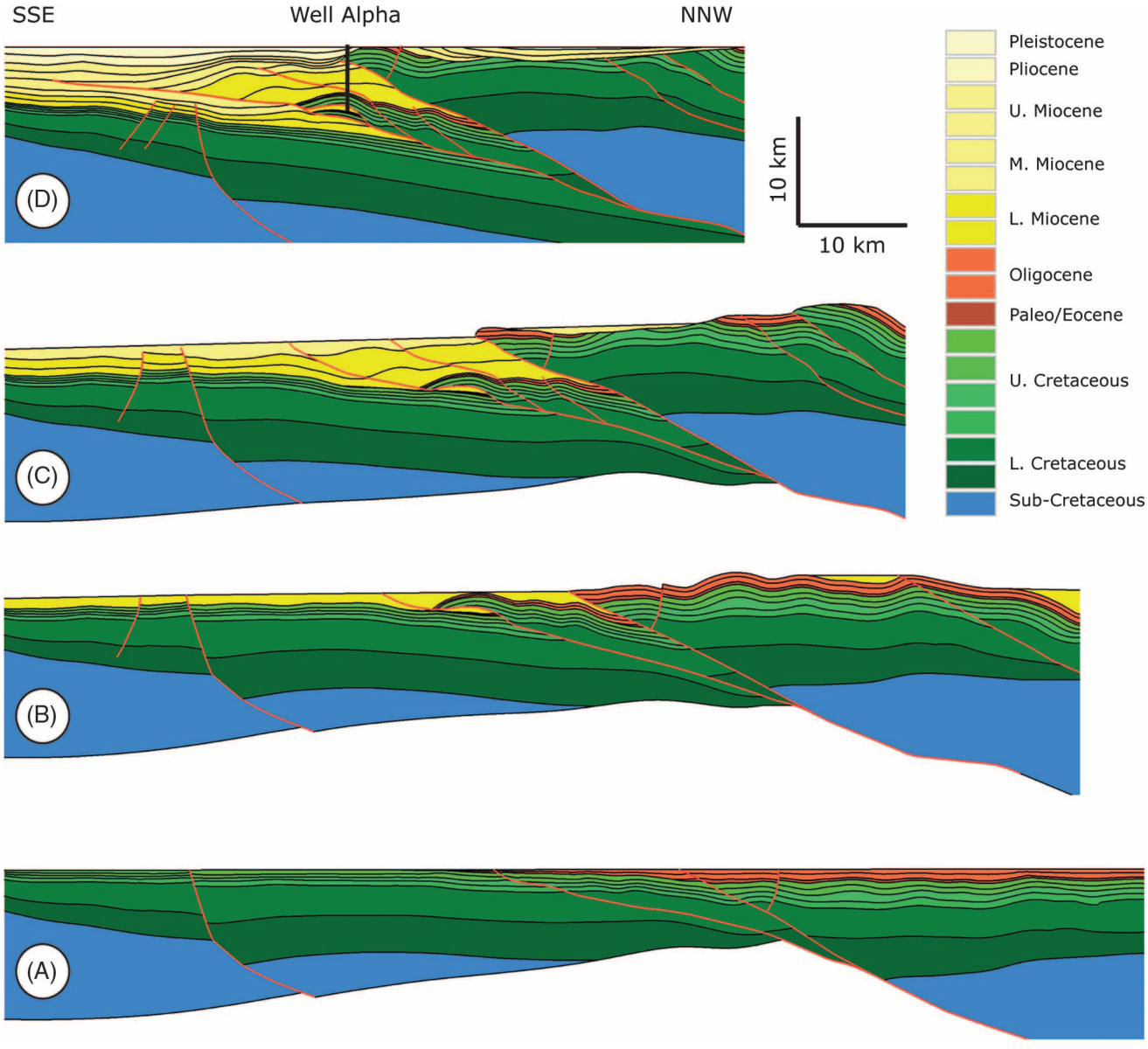

Figure 3. Structural evolution of the Monagas fold and thrust belt demonstrated by structural restoration: (A) Passive margin stage (until 23 Ma). (B) Early compression stage (21 Ma). (C) Late compression stage (12 Ma). (D) Present day. For details, see text.

we assumed a constant initial TOC of 6 wt% and an initial HI of 500 mg HC/g TOC. However, because initial TOC and HI were estimated from present-day measured values, these initial values are highly uncertain. In addition, there is both lateral and vertical variability within the layer; even though locally very high source rock potential is likely to occur, a bulk TOC and HI need to be assigned to the model cells. For these reasons, several models with different initial TOC have been run, and their sensitivity to the modeled charge is discussed below. Faults were set open to fluid flow in the course of their main kinematic activity, which is estimated by fault displacement analysis of the structural restoration models. After their main activity phase, faults are assumed to be closed. Fault permeability was also a varying parameter in the sensitivity analysis discussed below. Thermal boundary conditions are given in Table 2. Surface temperature ranges between 23 and 30°C (73.4 and 86°F) through geologic time, with a present-day average temperature of 28°C (82.4°F). These temperatures at sea level have been corrected

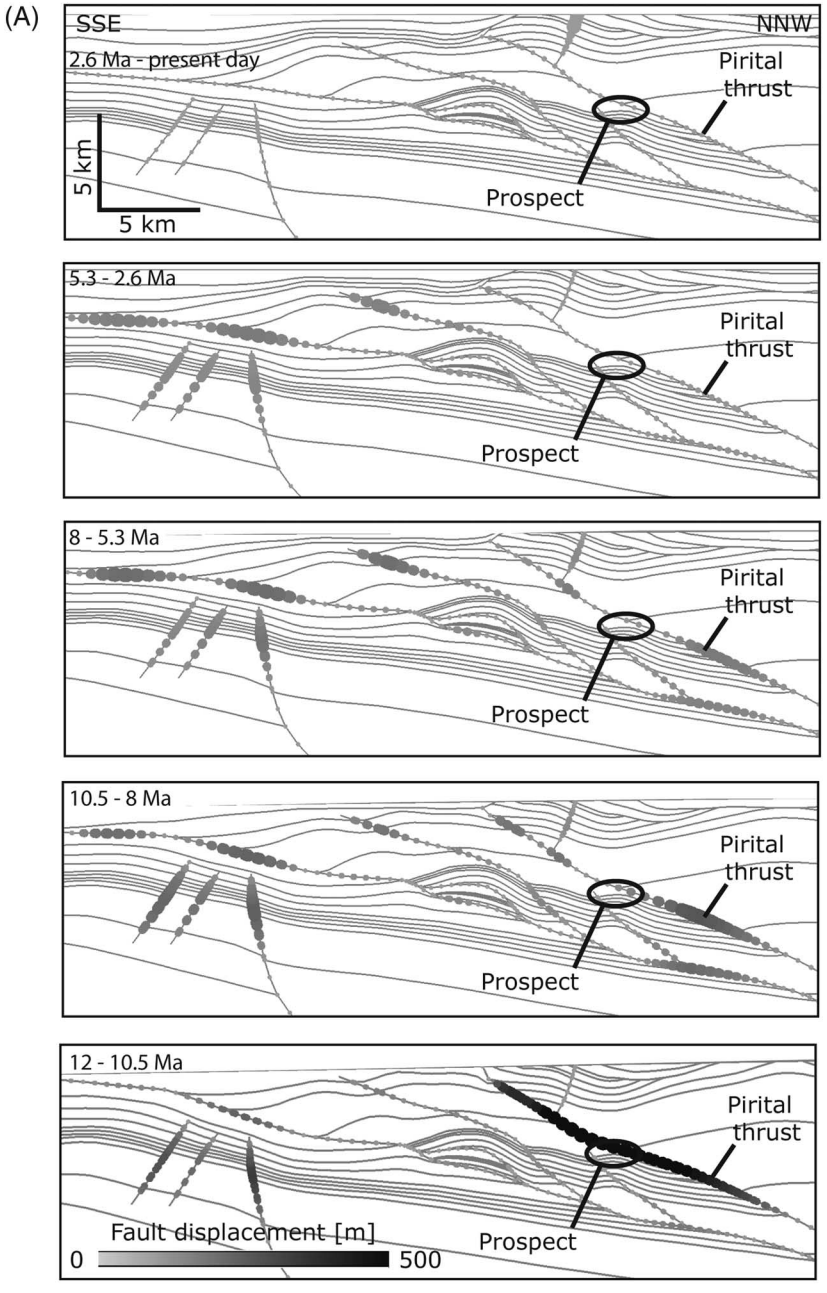

Figure 4. Fault displacement from late Miocene to present day for all faults on restored cross sections (A) and for the Pirital thrust only (B). Black and white shading and size of points show magnitude of displacement in meters.

Table 1. Basin and Petroleum System Modeling (BPSM) Input Parameters: Geologic Ages and Lithologies

Age (Ma)	Geologic Time	Facies	Density (kg/m^3)	Initial Porosity (%)	Compressibility (GPa^{-1})		Permeability (log mD)		Thermal conductivity (W/m/K)		Heat capacity (kcal/kg/K)	
					max.	min.	at 1% por.	at 25% por.	at 20°C	at 100°C	at 20°C	at 100°C
0												
	Pleistocene	Las Piedras sandstone	2720	41	27.47	1.15	−1.8	3	3.95	3.38	0.2	0.24
		Las Piedras shale	2700	40	403.27	4.03	−8.52	−3	1.64	1.69	0.21	0.24
2.6												
	Pliocene	Las Piedras sandstone	2720	41	27.47	1.15	−1.8	3	3.95	3.38	0.2	0.24
		Las Piedras shale	2700	40	403.27	4.03	−8.52	−3	1.64	1.69	0.21	0.24
5.3												
	upper Miocene 2	La Pica sandstone	2720	41	27.47	1.15	−1.8	3	3.95	3.38	0.2	0.24
		La Pica shale	2700	40	403.27	4.03	−8.52	−3	1.64	1.69	0.21	0.24
		Morichito shale	2700	40	403.27	4.03	−8.52	−3	1.64	1.69	0.21	0.24
8												
	upper Miocene 1	La Pica sandstone	2720	41	27.47	1.15	−1.8	3	3.95	3.38	0.2	0.24
		La Pica shale	2700	40	403.27	4.03	−8.52	−3	1.64	1.69	0.21	0.24
		Morichito basal sandstone	2715	48	121.42	1.87	−3.48	1.5	3.17	2.84	0.2	0.24
10.5												
	middle Miocene 2	Carapita sandstone	2715	48	121.42	1.87	−3.48	1.5	3.17	2.84	0.2	0.24
		Carapita shale	2705	63	309.32	3.31	−6.84	−1.5	2.04	2.01	0.2	0.24
12												
	middle Miocene 1	Carapita shale	2705	63	309.32	3.31	−6.84	−1.5	2.04	2.01	0.2	0.24
15												
	lower Miocene 2	Carapita shale	2705	63	309.32	3.31	−6.84	−1.5	2.04	2.01	0.2	0.24
19												
	lower Miocene 1	lower Carapita shale	2700	70	403.27	4.03	−8.52	−3	1.64	1.69	0.21	0.24
23												
	Oligocene 2	Merecure platform sandstone	2715	48	121.42	1.87	−3.48	1.5	3.17	2.84	0.2	0.24
27												
	Oligocene 1	Merecure platform sandstone	2715	48	121.42	1.87	−3.48	1.5	3.17	2.84	0.2	0.24

33.9												
	Paleo/Eocene	Vidono sandstone	2720	41	27.47	1.15	−1.8	3	3.95	3.38	0.2	0.24
		Caratas basinal shale	2700	70	403.27	4.03	−8.52	−3	1.64	1.69	0.21	0.24
65.5												
	upper Cretaceous 4	San Juan sandstone	2720	41	27.47	1.15	−1.8	3	3.95	3.38	0.2	0.24
74												
	upper Cretaceous 3	San Antonio siltstone (SOURCE ROCK)	2710	55	104.22	2.12	−6.28	−1	2.01	1.96	0.23	0.26
82.5												
	upper Cretaceous 2	San Antonio siltstone (SOURCE ROCK)	2710	55	104.22	2.12	−6.28	−1	2.01	1.96	0.23	0.26
91												
	upper Cretaceous 1	Querecual mudstone (SOURCE ROCK)	2700	70	403.27	4.03	−8.52	−3	1.64	1.69	0.21	0.24
99.6												
	lower Cretaceous 2	undiff lower Cretaceous (30% Lst50%Sst%20Sh)	2722	45	94.45	1.41	−3.34	1.74	3.05	2.75	0.2	0.23
122												
	lower Cretaceous 1	undiff lower Cretaceous (30% Lst50%Sst%20Sh)	2722	45	94.45	1.41	−3.34	1.74	3.05	2.75	0.2	0.23
145.5	sub-Cretaceous 2	undiff sub-Cretaceous (50%Sh50%Sst)	2710	55	215.37	2.59	−5.16	0	2.55	2.39	0.2	0.24
251												

Table 2. Basin and Petroleum System Modeling (BPSM) Input Parameters: Thermal Boundary Conditions

	Sediment/Water Interface Temperature (°C)			
Age (Ma)	min	max	Age (Ma)	Basal Heat Flow (mW/m^2)
0	28	28	0	42
2.6	28	28	30	60
5.3	7.6	23	34	70
8	18.4	23.1	50	50
10.5	6.2	23.3	107	60
12	3.1	23.8	145.5	80
15	5	24.2	260	60
19	5	24.7		
23	23.4	25		
27	7.8	23.5		
33.9	9.4	23.6		
65.5	14.6	28.3		
145.5	14.8	28.7		
255	5	23.9		

by the influence of the paleowater depth using the approach of Wygrala (1989). Because of the high topographic elevation of approximately 3500 m (11,500 ft), the maximum altitude during the past compressional phase, we adjusted the model, taking into account a temperature decrease of 6°C/km (3.3° F/1,000 ft) related to the paleoaltitude. This results in a difference of up to 20°C (36°F) compared to sea-level temperature. We then assigned the adjusted sediment/water interface temperatures to the model as the upper thermal boundary condition. At the base of the model, we assigned a heat flow ranging from 42 to 80 mW/m^2 through geologic time. The highest heat flow is assumed during the rifting event, before the basin cooled as a passive margin. A thermal event in the Eocene, detected by fission track analysis (Locke and Garver, 2005; Perez de Armas, 2005), has been addressed by a second peak before a second cooling phase. For uncertainty analysis, basal paleo-heat flow has been varied within geological meaningful ranges and the thermal calibration data has been honored as much as possible.

Modeling Results

Basin and petroleum system modeling can be divided into simulation of the physical parameters within a basin, such as pressure and temperature (basin modeling), and the subsequent evolution of the source rocks and their derived hydrocarbon compounds (petroleum systems modeling). In the following sections, we use this subdivision to describe the BPSM results: compaction modeling, thermal modeling, and charge history. It is important to state that these are predictions based on forward modeling as just described. The results are compared and calibrated to actual measurements and observations, where available.

Compaction Modeling

Figure 5 presents an extraction of the modeled results at the location of Well Alpha in the Furrial Trend. In the absence of direct calibration data for pore pressure, we undertook a sensitivity analysis to test the different scenarios. Using the model, we tested how pore pressure in the main reservoir of the Furrial Trend reacts to changes in fault and seal-rock permeability. In a first step, fault permeability has been evaluated. Faults were assumed open during the main fault activity phase and closed afterward. In addition, we performed several variations from that base case scenario. Figure 5A shows the effect of two end-member scenarios on pore pressure within the main reservoir of the Furrial Trend (Santa Barbara field) in which faults have been modeled to be either open or closed since their formation. A third scenario consists of thrust faults that are open during the compressional phase (from 15 Ma on), and closed afterward (from 10.5 Ma on). This scenario has been chosen as the "master scenario" because it results in overpressure of 23 MPa, which is in the range of pressure reported in similar structures of the Furrial Trend by Schneider et al. (2004). In addition, this pressure scenario matches the calibration data for porosity (Figure 5B).

The 2D distribution of modeled overpressure at present day is shown in Figure 6A. Apart from important overpressure in the Querecual Formation, the allochthon is almost normally pressured. The thrust wedge is overpressured, especially in the low-permeability Carapita Formation. Although

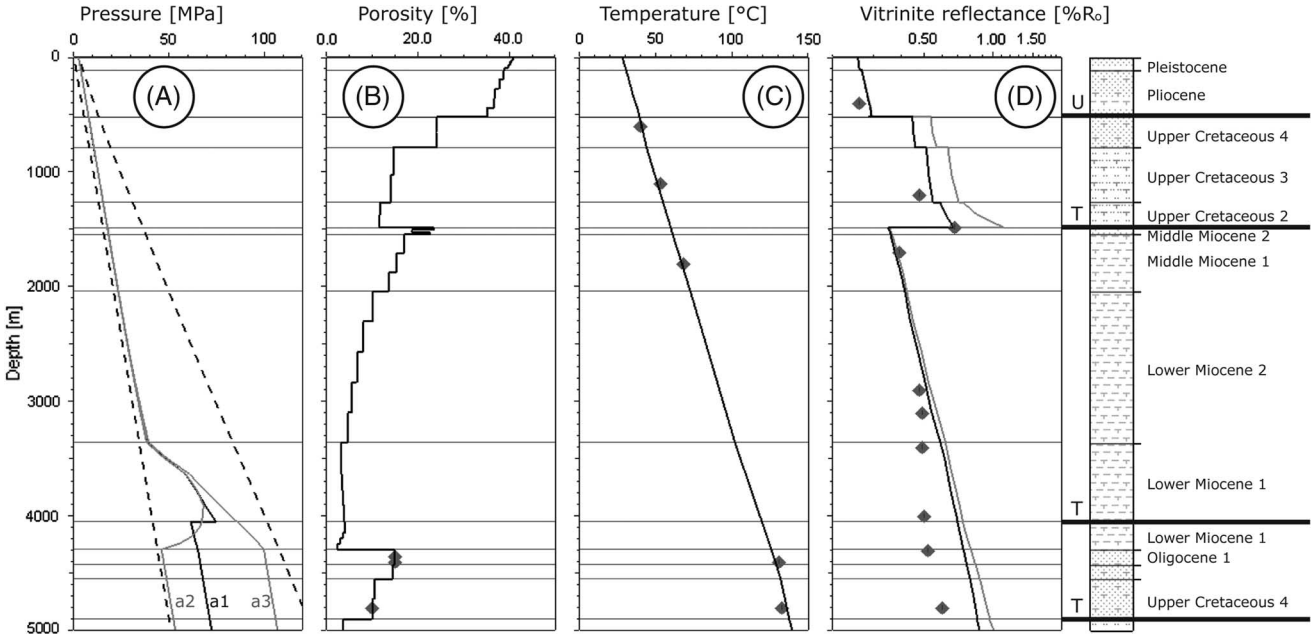

Figure 5. Plots of one-dimensional model output and available calibration data for Well Alpha (Table 3); (A) Dotted lines are hydrostatic and lithostatic pressures, continuous lines are pore pressure; the master scenario is in black (a1: faults closing at 10.5 Ma) and additional scenarios in gray (a2: open faults; a3: closed faults); (B) modeled porosity; (C) borehole temperature, and (D) R_o. The black line shows the master scenario and the gray line the alternative high-heat-flow scenario. Bold lines in the stratigraphic column are thrusts (T) and unconformities (U).

Table 3. Calibration Data for Well Alpha (Porosity, Temperature, R_o)

TVD (m)	Porosity (%)	TVD (m)	Corrected Temperature (°C)	TVD (m)	Vitrinite Reflectance (%R_o)
4350	15	600	40	400	0.26
4400	15	1100	53	1200	0.48
4800	10	1800	68	1485	0.68
		4400	131	1700	0.39
		4800	133	2900	0.48
				3100	0.49
				3400	0.49
				4000	0.5
				4300	0.52
				4800	0.6

the autochthon is highly overpressured, close to normal hydrostatic pressures are simulated in the foreland basin. The discussed model assumption of closed faults in the postcompressional phase results in a regional pressure compartmentalization.

The simulated pressure evolution through geologic time can be seen in Figure 7A. A time extraction of a source rock cell in the thrust wedge shows a sudden increase of both lithostatic and hydrostatic pressures that is a consequence of the tectonic burial load associated with the thrusting. In addition, the modeled pore pressure buildup, even though delayed in time, can be directly linked to the thrust event. It can be clearly seen that the timing of fault permeability directly impacts changes in the present-day pore pressure. The earlier the faults close, the more overpressure, generated by the massive syntectonic sedimentation, is kept until present day, given adequate sealing lithologies are present. The present-day overpressure is modeled as14 MPa when the faults are

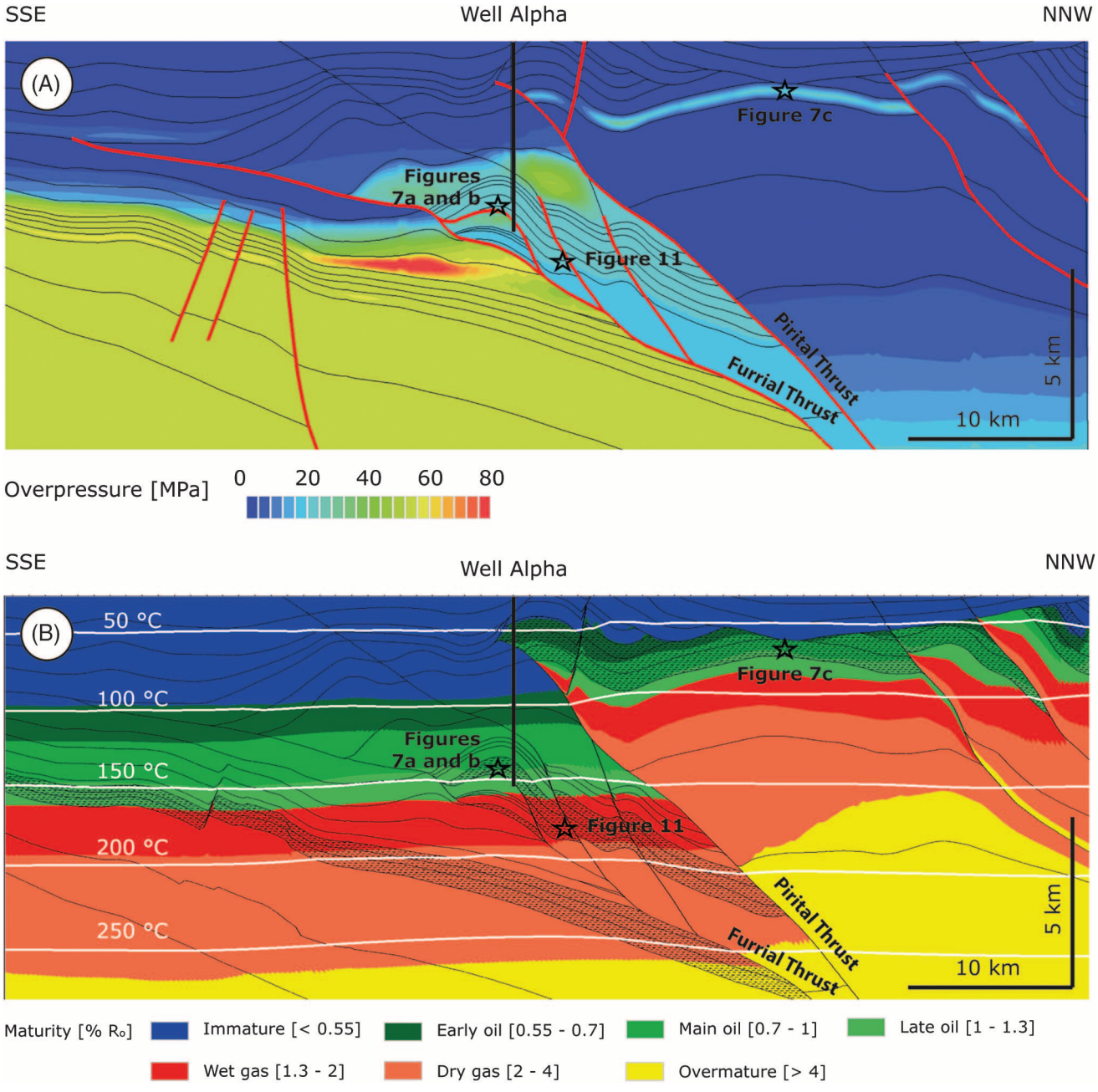

Figure 6. Two-dimensional model at present day with (A) modeled overpressure and (B) modeled thermal maturity and isotherms. Source rocks marked by lithology pattern.

open since 8 Ma, as 23 MPa for 10.5 Ma, and as 37 MPa for 12 Ma. Compared to this order of magnitude, changes in the permeability of the overlying Carapita shale are negligible for the pore pressure. Therefore, the controlling parameter for pore pressure in the main reservoir of the Furrial trend is assumed fault permeability and resulting lateral connectivity, rather than the permeability of the seal rock.

Thermal Modeling

Modeled temperature and thermal maturity (Figure 5C, D) have been calibrated with available well data. Some discontinuities in the modeled R_o trend are noted (Figure 5D): The upper kinks (e.g., base Pliocene) are related to unconformities with associated erosion, and the lower one (base Upper Cretaceous) is due to the well penetrating a reverse

fault displacing mature rocks upon less mature ones (see Figure 6B for 2D view). There is a mismatch between the modeled R_o trend and the data in the deeper part of the well. In the Oligocene rocks, the modeled temperature is too low (2°C or 3.6°F), whereas the modeled R_o is too high (up to 0.2% R_o). Any attempt to reduce the modeled R_o (e.g., by changing thermal conductivity of the Miocene Carapita Formation) also results in a lower modeled present-day temperature. Therefore, the thermal scenario used for this calibration is a trade-off between matching present-day temperature and R_o (using the kinetics of Sweeney and Burnham, 1990). The basal heat flow assumed in the master scenario (Table 2) results in a modeled present-day surface heat flow ranging from 37 mW/m^2 in the southern part of the thrusts to 52 mW/m^2 in parts of the uplifted area. At the same depth, the allochthonous northern part is thermally more mature than the southern autochthon (Figure 6B) because of the recent uplift. Locally inverted trends around the thrusts can be observed; for example, at the location of Well Alpha (see Figure 5D). In the autochthon, the Upper Cretaceous source rocks are entirely in the oil or even gas window at present day because of the Neogene tectonic loading and synorogenic deposition. In the northern allochthon, most of the Upper Cretaceous source rocks have been in the oil window in the past. The modeled thermal maturity is in good agreement with the regional maturity suggested by Summa et al. (2003).

Similar to the pressures, the thrusting also affects the modeled temperature and R_o. In the thrust wedge, a direct relationship exists between the thrusting and the increase of temperature and maturity. The thrusting is the trigger for source rocks entering the oil window within the thrust wedge (Figure 7B), and the present-day thermal maturity has been reached since the last 10 Ma. Although this recent thermal history can be considered as relatively well constrained by the measured R_o in the calibration well, this does not apply to the past. In this thrusted area, any thermal maturity reached prior to the thrusting onset has been "overprinted," and therefore no thermal calibration is possible for this period. However, the Cretaceous source rocks were not buried deeply during the passive margin phase, and even very hot scenarios (basal heat flow of 100 mW/m^2) do not significantly change their maturity (Figure 7B). In the uplifted allochthon, several wells show low (0.3%) to moderate (1%) measured R_o (Parra et al., 2011). Because the allochthon experienced its maximum burial and the highest temperatures during the passive margin phase, these maturity levels can be assumed as representative of the maturity prior to the compression. In contrast to the thrust wedge, the consequence of the thrusting is inverse for the allochthon (Figure 7C) as the hanging wall is uplifted and the accompanying erosion removes the overburden. The highest temperatures are simulated to have been reached just before the thrusting event. Then temperature decreased, and R_o stagnated, leaving the source rocks in the early mature zone until present day. The assumption of a regionally relatively homogeneous thermal field during the cooling phase of the passive margin in combination with the relatively low maturities measured in the uplifted allochthon makes the hot heat-flow scenario unlikely. However, a laterally varying heat flow cannot be excluded, and the consequently hotter paleoheat flow would have led to much higher temperatures prior to compression, resulting also in a higher present-day maturity level (1.4%), despite the uplift (Figure 7C). Any variations of basal heat flow during the rift period (Late Jurassic to Early Cretaceous) occurred too early to affect the maturity of the source rocks deposited during the late Cretaceous.

Charge History

After calibration of the basin's physical environment, the evolution of the petroleum systems was modeled. Hydrocarbon generation was simulated through geologic time using the activation energy distribution of the assigned source rock kinetics. From the moment of hydrocarbon expulsion onward, secondary migration was modeled using the invasion percolation method (Wilkinson, 1984). It takes into account the geometry, overpressure gradient, and capillary entry pressures of the rocks, which are opposed to the buoyancy of the migrating oil and gas. Figure 8 shows the time evolution of the total study area, and Figure 9 focuses on the thrust wedge. As already mentioned, the described charge history is based on forward modeling. It is consistent

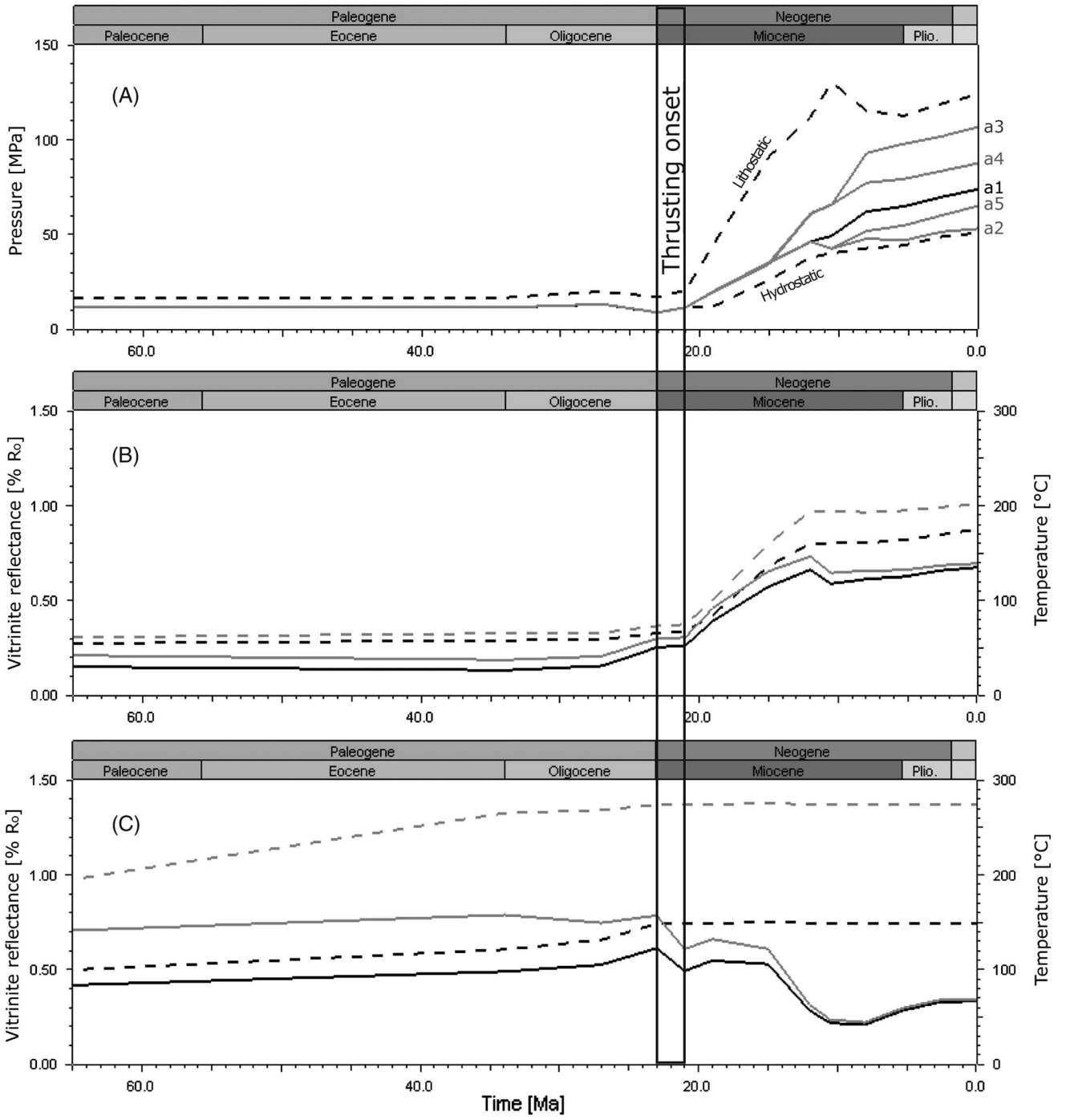

Figure 7. Time extractions (see Figure 6 for location): (A) Pressure development through geologic time for a source rock in the vertical continuity of Well Alpha. Dotted lines are hydrostatic and lithostatic pressures, continuous lines are pore pressure; the master scenario is in black (a1: faults closing at 10.5 Ma) and additional scenarios in gray (a2: open faults; a3: closed faults; a4: faults closing at 12 Ma; a5: faults closing at 8 Ma). (B) Temperature (continuous lines) and R_o (dotted lines) through geologic time for a source rock in the vertical continuity of Well Alpha; the black line shows the master scenario and the gray line the alternative high-heat-flow scenario. (C) Temperature (continuous lines) and R_o (dotted lines) through geologic time for a source rock in the uplifted allochthon; the black line shows the master scenario and the gray line the alternative high heat flow scenario.

with the modeled compaction and thermal history, and therefore shows one scenario that explains the charge of the Santa Barbara field and the foreland basin. Simplifications are inherent to any such workflow and shall be considered when analyzing the modeling results.

Passive Margin Phase—Mesozoic to Oligocene

Modeling results indicate that already during the Late Cretaceous, any Jurassic source rocks potentially deposited in the northern part of the section (Summa et al., 2003) have reached temperatures of more than 200°C (392°F) and corresponding high levels of maturity. However, the temperature at the base of the Querecual Formation (Upper Cretaceous) was less than 100°C (212°F), leaving the kerogen immature. The source rock became effective only during late Eocene, with temperatures of up to 120°C (248°F) and a (reactive kerogen to hydrocarbon) transformation ratio (TR) of more than 20% in the deeper distal part of the passive margin. Oil was quickly expelled, migrated vertically, and seeped to the surface because of the general lack of seals in the overburden. During the Oligocene, the time of deposition of the Merecure reservoir sandstones in the southern platform, this situation did not change apart from increased transformation in the deeper basinal part of the passive margin.

First oil accumulations are modeled in the Vidoño sandstones in the basinal part in the late Oligocene (Figure 8A), in which the base of the Querecual Formation shows TRs of up to 60% at around 130°C (266°F). In the proximal part, there is no hydrocarbon generation. Although there is a general northward tilting slope, no southward migration from the distal margin is modeled; this has been checked using different migration methods including Darcy flow, with scenarios of continuous intrasource carrier beds. This is in contrast to the studies from Gallango and Parnaud (1995) and Schneider (2003), who suggested lateral migration at that stage. The difference could be explained by the presence of a regional top seal in their models. However, our model suggests that the shallow rocks do not have sufficient sealing capacity to allow lateral hydrocarbon migration. During the passive-margin phase, the basin was normally pressured (Figure 7A), and simulated stresses have not yet resulted in any fracturing at that stage.

Main Compressional Phase—Early to Middle Miocene

With the onset of compression during early Miocene (Figure 8B), both the Pirital and Furrial thrusts were formed, and the northern distal part of the passive margin was rapidly uplifted. Important overpressures as well as mechanical rock failure, both the result of the rapid uplift, are simulated in the allochthon. Despite this uplift, the kerogen-to-hydrocarbon transformation continued, and the rate even increased locally close to the footwall cutoffs and where synorogenic deposition provided rapid overburden loading. Oil accumulations are modeled in the freshly created anticlines.

The tectonic–sedimentary wedge between the two main thrusts experienced very rapid burial. In fact, the Upper Cretaceous source rocks were brought into depths where temperatures were as high as 185°C (365°F) at 19 Ma and 225°C (437°F) at 15 Ma. Especially close to the cutoff of the Pirital thrust, they very quickly reached a high maturity at 19 Ma and reached full transformation in most places at 12 Ma. The expelled hydrocarbons migrated into the sandstones of the Merecure Formation, which were sealed by the Carapita Formation. The charge toward a series of recent anticlines is modeled by the fill-to-spill mechanism from north to south (Figure 9C, D). After the first oil fill, the northern prospect quickly received a local gas charge; the central structure contained mainly oil. Note the presence of a lateral seal that is due to sand–shale juxtaposition. The southernmost structure, which forms the Santa Barbara field today, was charged by oil only at 15 Ma (Figure 9D).

The generated hydrocarbons in the southern autochthon were leaking to the surface until the Carapita Formation was compacted enough to hold some of them (Figure 8C). At 12 Ma, the wedge source rocks were mostly spent, but expulsion was still ongoing. Important rock failure is modeled to have occurred in the thrusted footwall, breaking the formerly sealing Carapita Formation (Figure 10). This is in good agreement with cemented hydraulic fractures observed in a few cores in the Carapita

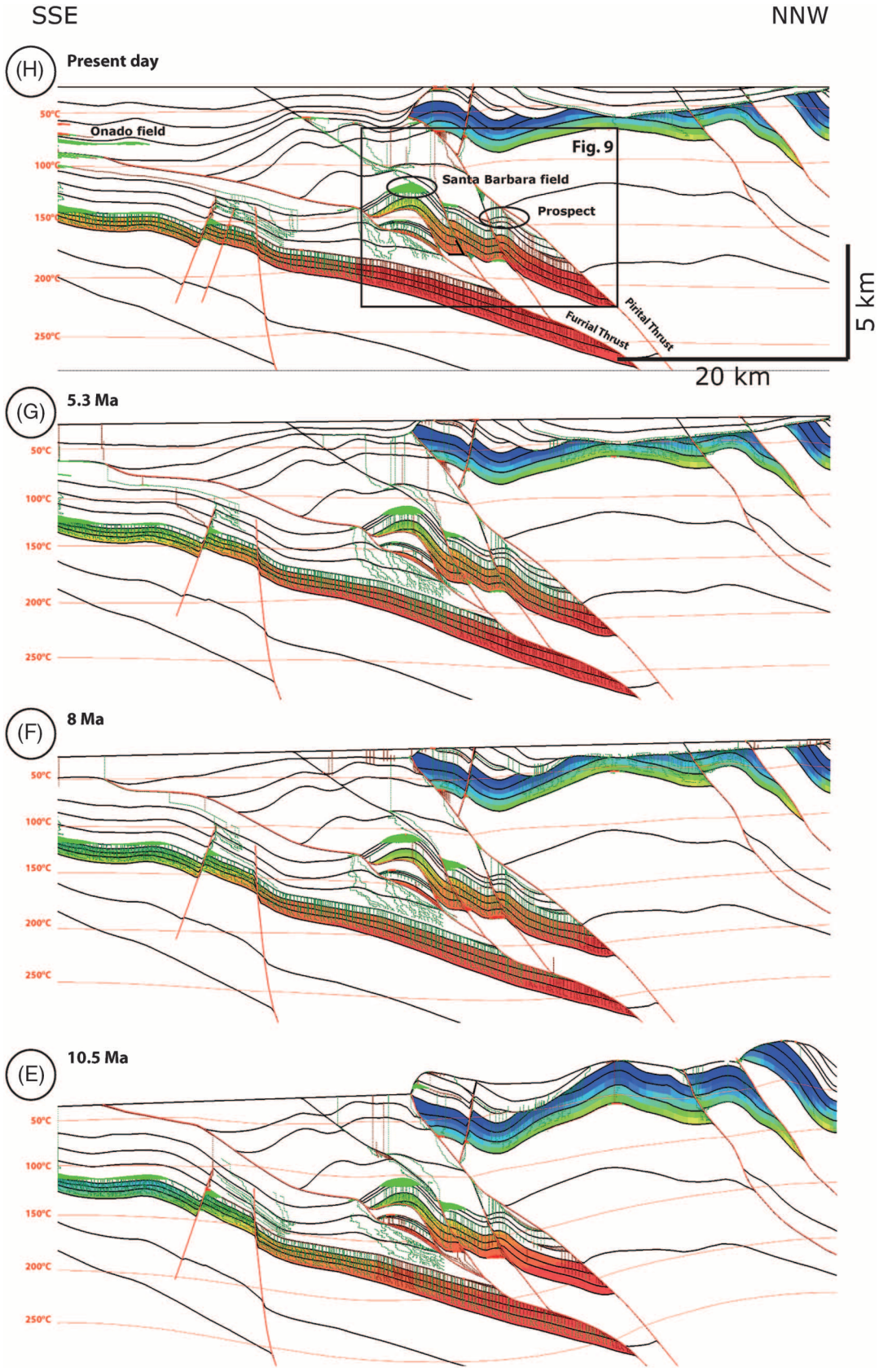

Figure 8. Two-dimensional model through geologic time (selected time steps only) with modeled transformation ratio for the source rock layers, isotherms, and liquid and vapor migration and accumulation.

shales from the Furrial Trend (Roure et al., 2005). This important fracturing event resulted in the destruction of the modeled accumulation (Figure 9E). Hydrocarbon generation and expulsion were also happening in the southern foreland basin at transformation ratios of up to 30%.

Late Compressional and Postcompressional Phase—Late Miocene to Present Day

The late compressional phase was marked by the partial destruction of the allochthonous petroleum systems by erosion (Figure 8E, F). Many traps disappeared and

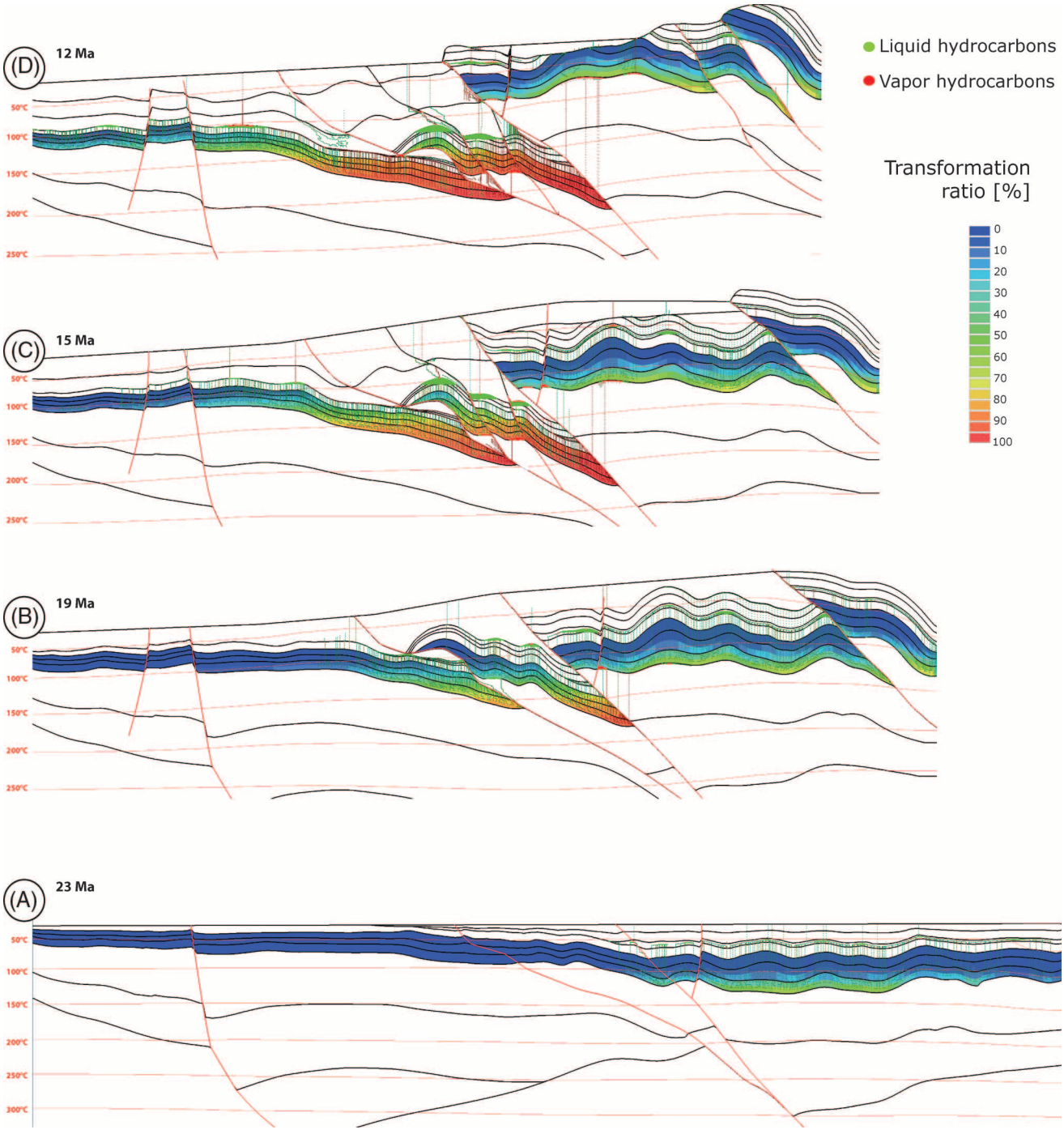

Figure 8. Continued.

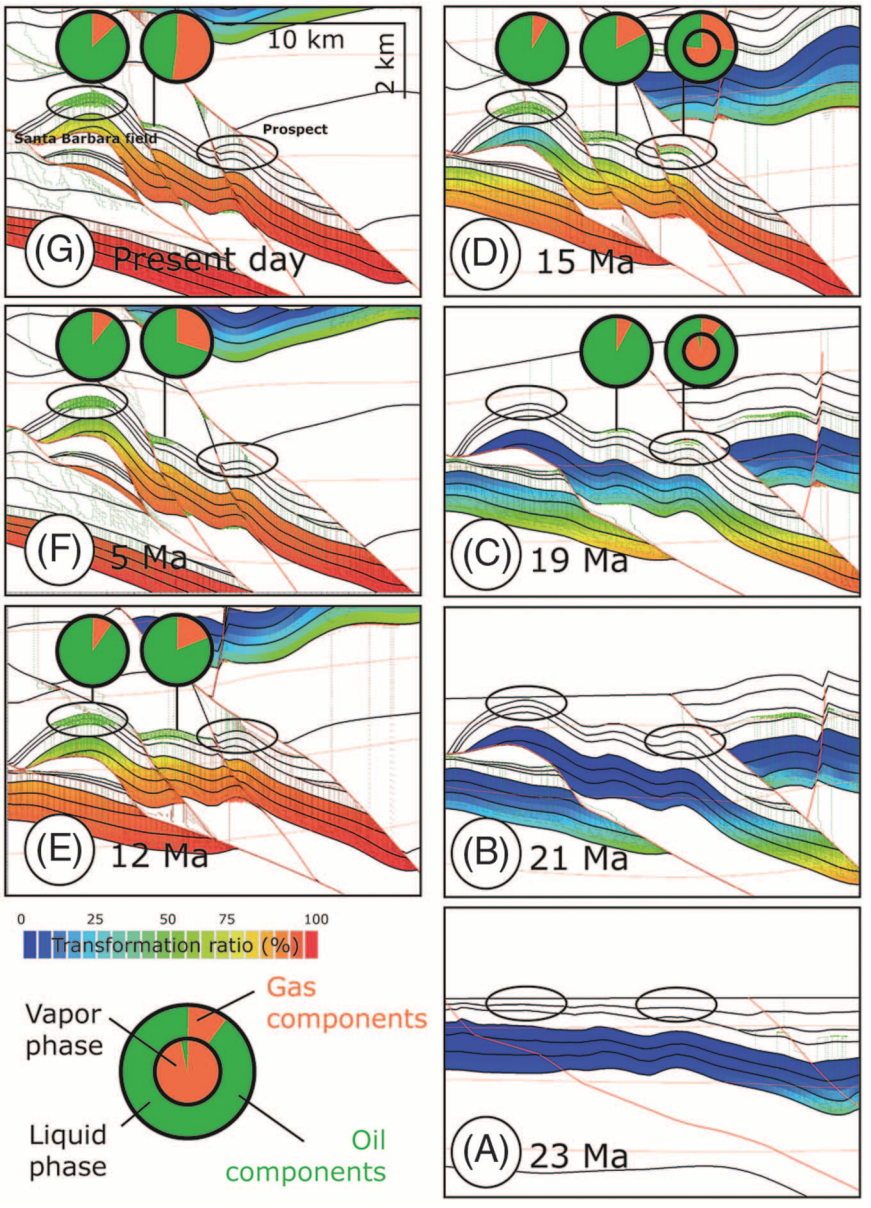

Figure 9. Detail of two-dimensional model through geologic time (see Figure 8), showing modeled transformation ratio for the source rock layers, isotherms, and liquid and vapor migration and accumulation. The Santa Barbara field and the prospect are shown by ellipses.

the hydrocarbon generation within the source rocks stopped. The erosion triggered an important sediment transfer toward the south, contributing to further burial and increased temperatures in the thrust wedge and the foreland basin. During late Miocene, the petroleum system in the wedge matured. An important northward tilting was triggered by flexural tectonic loading and the loading of syntectonic sediments (Summa et al., 2003). In combination with the presence of an effective regional top seal, the compacted Carapita Formation allowed a change from dominantly vertical migration into lateral migration. First, accumulations are modeled in the Neogene synorogenic sequence reservoirs in the south, and important southward migration toward the foreland basin started (Figure 8G). These trends continued through Pliocene and Pleistocene times to present day, filling the Onado field (Figure 8H) and other known fields in the south (Figure 1A) of the Eastern Venezuela Basin.

Prospectivity

We modeled the charge of the Santa Barbara field in the Furrial Trend and of the Onado field in the foreland basin (Figure 8H). Other prospects in the thrust wedge were also investigated. The structure called

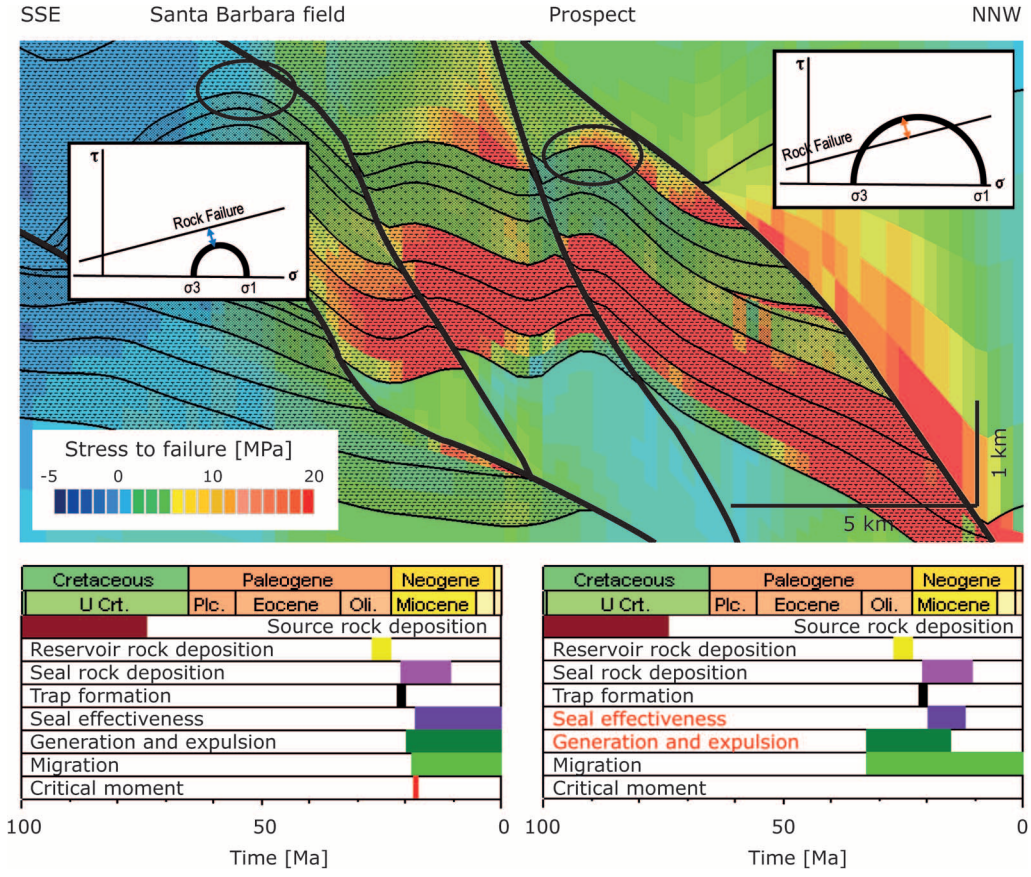

Figure 10. Two-dimensional model (at 12 Ma) with modeled stress to failure, Mohr circles (with σ standing for normal stress and τ for shear stress), and petroleum system events charts for the Santa Barbara field (left) and the prospect (right). Model predicts rock failure in the prospect from about 12 Ma. For further details, see text.

"prospect" (Figure 9G) looks similar to that of the Santa Barbara field because both are anticlines and the reservoir and seal formations are the same. However, they differ in several aspects. First, the prospect is in the vicinity of the Pirital thrust, which presents a high risk of impacting the seal integrity. The prospect location is directly below the area where we presume the maximum of late tectonic activity occurred (Figure 4). As modeled, the Carapita Formation, the seal of the prospect, was already brittle when this deformation occurred. Calculated stresses also predict rock failure from 12 Ma onward (Figure 10). Even though charge continued, our model suggests continuous leakage of the structure (Figure 9E–G). The second major difference is that the source rock in the fault block of the prospect is modeled to have already started generating and expelling hydrocarbons during the Oligocene and early Miocene (Figure 9A), before the trap formed and the seal became effective (Figures 9C, 10). Even though generation, expulsion, and migration continued after trap formation, the prospect was not charged with the earlier expelled oil. In addition, the present-day maturity of the source rocks within the prospect's fault block is higher than in the source rocks within the tectonic block of the Santa Barbara field, potentially indicating expulsion of more gas. A south–north trend can be seen on the modeled accumulation composition, with more gas toward the allochthon (Figure 9). The modeled composition of the prospect prior to seal failure was much richer in gas than in the neighboring Santa Barbara field (Figure 9D). In fact, simulation scenarios with unbreached seals resulted in accumulation of predominantly gas. The combination of both seal integrity and charge composition concerns makes this a risky prospect. In addition, potential diagenetic fluids related to the fault fluid flow might have altered the reservoir quality.

Apart from the Onado oil field, only minor accumulations are modeled in the southern Neogene synorogenic sequence. The proportion of gas is higher than in the Furrial trend. The accumulations at the southern model edge are a modeling artifact, representing hydrocarbons (mainly oil) that in reality are thought to have charged the southern foreland basin (from mid to late Miocene times to present day). However, parts of the migrated oil and gas could have been trapped in the Upper Cretaceous San Juan Formation south of the horst structure.

The potential for conventional hydrocarbon accumulations in the allochthon is very limited by the important fracturing that occurred during the uplift period. The basal sandstones of the Morochito piggyback basin north of the Pirital thrust are not charged in our 2D model because of the absence of structural traps. Nevertheless, there is a potential for stratigraphic traps to have been charged as migration through the basin occurred. However, seal strength might be critical at this low-compaction stage. The same applies for the Las Piedras Formation. We think there might be potential for shale oil because the Querecual Formation is at shallow depths but shows maturity within the oil window. From the thermal maturity point of view, any potential Jurassic source rocks, as discussed by Summa et al. (2003), might be a gas source or shale gas target.

UNCERTAINTY ANALYSIS

There is often significant uncertainty in basin geometry and depth of stratigraphic horizons based on uncertain seismic interpretation and velocity models (Kukla et al., 2000; Brandes et al., 2008; Baur et al., 2010). Restoring of present-day geometries to obtain paleogeometries adds further uncertainty. Additional uncertainty is related to thermal boundary conditions such as paleoheat flow (Beha et al., 2008), and to geochemical properties such as source rock characteristics and petroleum generation kinetics, and calculation of biodegradation and petroleum density (Blumenstein et al., 2008). In addition to the pore pressure and thermal sensitivity analysis just described, we varied initial TOC within a range of 2% to 10%. A variation of initial TOC obviously directly scales the amount of initial kerogen available for transformation into hydrocarbons. Neither the charge volume nor composition of the Santa Barbara field, nor the wedge prospects are significantly sensitive to variation of initial TOC; these traps are filled to spill in each scenario. However, the amount of hydrocarbons charging the foreland basin (e.g., the Onado field) is reduced in the case of low initial TOC. A high initial TOC only increased the modeled amount of surface seepage. The sensitivity of the initial HI is analogous to the sensitivity of the initial TOC.

In addition to the more classical uncertainty and sensitivity analysis described, we focused on quantitative analysis of the decompaction uncertainty when performing structural restoration. This uncertainty is particular to the applied workflow of using structurally restored paleogeometries in BPSM. Note that this uncertainty is significantly lower when using the backstripping method with the optimization algorithms discussed. One method to analyze the adequacy of the decompaction method is comparison of the output rock matrix mass balance. In the backstripping approach, the rock matrix mass is kept constant of a model cell with a simulated decrease in porosity controlled by compaction laws and the corresponding reduction of the layer thickness. When using fixed paleogeometries from structural restoration, the cell thickness is imposed. However, the decrease in porosity is calculated, and the mass is adapted to fit the imposed cell thickness. That means that the rock matrix mass is constant only if ideal decompaction has been applied.

Figure 11A shows the percentage variation from the present-day matrix mass (100%) of a given source rock cell through geologic time. The dotted line represents the ideal case with constant rock matrix mass. We used two end-member decompaction scenarios to describe the decompaction-related uncertainty that is introduced when fixed paleogeometries replace backstripping: idealized hydrostatic decompaction assuming no overpressure and idealized lithostatic decompaction assuming no effective stress (no decompaction, resulting in constant cell thickness through time). In the latter case, with decreasing porosity during compaction, the rock matrix mass

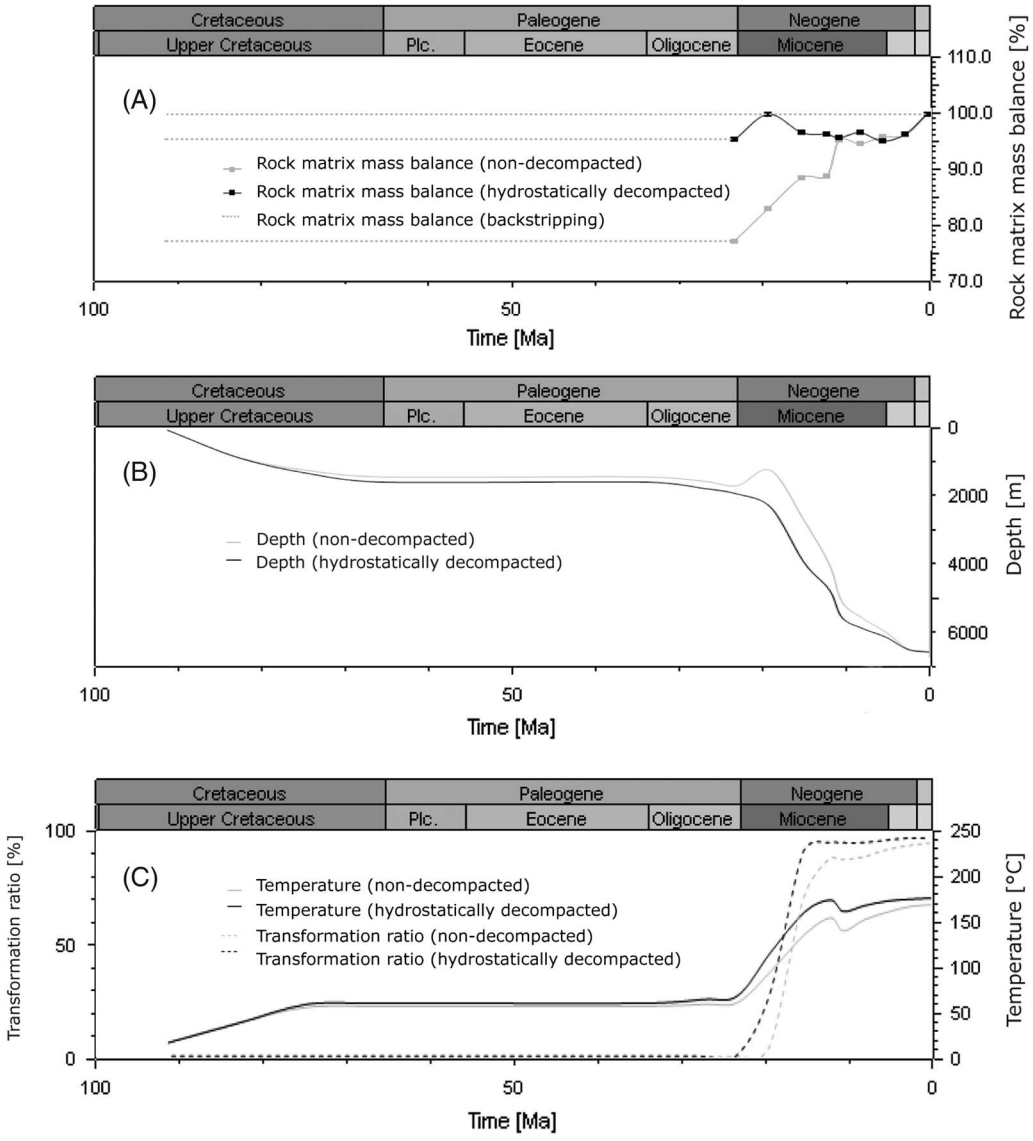

Figure 11. Time extractions for comparison of two end-member decompaction scenarios (see Figure 6 for location): (A) Rock matrix mass conservation through geologic time. (B) Source rock burial depth through geologic time. (C) Temperature and transformation ratio through geologic time.

increases until it reaches the present-day mass. In other words, rock mass matrix has been highly underestimated in the past (in this particular case by more than 20%). This is a source rock, so the kerogen mass decreases by the same factor. This yields an underestimation of more than 20% in TOC! Note the rock matrix mass is constant for time steps prior to 23 Ma, in which backstripping optimization could be performed toward the earliest paleogeometry. For the second end-member scenario of idealized hydrostatic decompaction, the rock matrix mass is nearly constant, which is a good decompaction adequacy indicator for that given cell in the model. However, the so-measured adequacy changes throughout the model. In some areas, the rock matrix mass has been underestimated by about 50% for nondecompacted paleogeometries; however, in the case of hydrostatic decompaction, values generally range from 80% to 120% of the present-day rock matrix mass. That means, in this particular case, that hydrostatic decompaction is more adequate (or less wrong) than no decompaction at all. The decompaction adequacy can be roughly correlated with pressure changes through geologic time.

Inadequate decompaction results in wrong depth for stratigraphic horizons in the paleogeometries. Figure 11B shows the burial depth of the same investigated source rock cell. We can see that during the passive margin phase, there is a slight difference in paleoburial depth for the two end-member scenarios. During the compressional phase, the difference changes dramatically, reaching more than 1000 m (3281 ft) in some places. Toward present day, both curves meet again, because the input to the two restoration scenarios was the same (identical present-day burial depth). This difference in compaction calculation has severe implications on the modeled temperature history and the kerogen-to-hydrocarbon transformation (Figure 11C). For an identical thermal framework in terms of modeling input parameters, temperature differences of up to 25°C (45°F) result in TR differences of more than 20% in the early compressional phase before TR values meet again for the present-day situation.

CONCLUSIONS

Structurally complex areas are attracting increasing interest in hydrocarbon exploration. Exploration risk can be substantially narrowed by analyzing the history of the basin and its petroleum systems based on structural evolution. We presented a further progress in technology that allows the integration of structural restoration and BPSM. This combined analysis is seen as a way forward to improve modeling in thrust belts with stacked stratigraphic sequences. Despite limitations of nonoptimized decompaction, which are added to the general uncertainty related to the individual methods, we modeled the charge and seal history of the Monagas fold and thrust belt in Venezuela. Calibrated porosity, temperature, and thermal maturity, as well as basin-scale stress, provided the regional framework through geologic time in which the petroleum systems evolved such that the charge of the known Santa Barbara and Onado fields and other trends could be understood. We discussed seal integrity of a potential exploration prospect by analyzing structural restoration-derived fault displacement through geologic time and an advanced stress forward simulation. The uncertainty of using decompacted or nondecompacted structural restoration has been assessed. It can have important influence on rock matrix mass balance through geologic time, paleogeometry, and paleoburial depth, and therefore affect paleotemperatures and paleomaturities. We conclude that decompaction assuming hydrostatic pressure is the best option in that particular case.

REFERENCES CITED

Alberdi, M., and E. Lafargue, 1993, Vertical variations of organic matter content in Guayuta Group (Upper Cretaceous), interior mountain belt, eastern Venezuela: Organic Geochemistry, v. 20, p. 425–436, doi: 10.1016/0146-6380(93)90091-O.

Athy, L. F., 1930, Density, porosity and compaction of sedimentary rocks: AAPG Bulletin, v. 14, p. 1–24.

Aymard, R., L. Pimentel, P. Eitz, P. Lopez, A. Chaouch, J. Navarro, J. Mijares, and J. G. Pereira, 1990, Geologic integration and evaluation of Northern Monagas, Eastern Venezuelan Basin, *in* J. Brooks, ed., Classic petroleum provinces: The Geologic Society (London), Special Publication v. 50, p. 37–53.

Baur, F., M. Di Benedetto, T. Fuchs, C. Lampe, and S. Sciamanna, 2009, Integrating structural geology and petroleum systems modeling—A pilot project from Bolivia's fold and thrust belt: Marine and Petroleum Geology, v. 26, no. 4, p. 573–579, doi: 10.1016/j.marpetgeo.2009.01.004.

Baur, F., R. Littke, H. Wielens, C. Lampe, and T. Fuchs, 2010, Basin modeling meets rift analysis—A numerical modeling study from the Jeanne d'Arc basin, offshore Newfoundland, Canada: Marine and Petroleum Geology, v. 27, p. 585–599, doi: 10.1016/j.marpetgeo.2009.06.003.

Beha, A., R. O. Thomsen, and R. Littke, 2008, Thermal history, hydrocarbon generation and migration in the Horn Graben in the Danish North Sea: A 2D basin modelling study: International Journal of Earth Sciences, v. 97, p. 1087–1100, doi: 10.1007/s00531-007-0247-2.

Blumenstein, I. O., B. M. Krooss, R. di Primio, W. Rottke, E. Müller, C. Westerlage, and R. Littke, 2008, Biodegradation in numerical basin modelling: A case study from the Gifhorn Trough, N-Germany: International Journal of Earth Sciences, v. 97, p. 1115–1129, doi: 10.1007/s00531-007-0272-1.

Brandes, C., A. Astorga, R. Littke, and J. Winsemann, 2008, Basin modelling of the Limón back-arc basin (Costa Rica): Burial history and temperature evolution of an island arc-related basin-system: Basin Research, v. 20, p. 119–142, doi: 10.1111/bre.2008.20.issue-1.

Carnevali, J. O., 1988, El Furrial oil field, northeastern Venezuela: First giant in foreland fold and thrust belts of western hemisphere: AAPG Bulletin, v. 72, 68 p.

Chevalier, Y., 1987, Contribution a l'etude géologique de la frontieré Sud-Est de la plaque Caraibe: Les zones internes de la chaine Sud-Caraibe sur le transect ile de Margarita-

Peninsule d' Araya (Venezuela): Ph.D. Université de Bretagne Occidentale, Brest, 494 p. (in French).

Erlich, R. N., and S. F. Barrett, 1992, Petroleum geology of the Eastern Venezuela foreland basin, *in* R. W. Macqueen and D. A. Leckie, eds., Foreland basins and fold belts: AAPG Memoir 55, p. 341–362.

Gallango, O., M. Escandon, M. Alberdi, F. Parnaud, and J.-C. Pascual, 1992, Hydrodynamism, crude oil distribution, and geochemistry of the stratigraphic column in a transect of the eastern Venezuela basin (abs.): Annual meeting of the Geological Society of America, Cincinnati, October 26–29, Abstracts with Programs, A214 p.

Gallango, O., and F. Parnaud, 1995, Two-dimensional computer modeling of oil generation and migration in a transect of the Eastern Venezuela basin, *in* A. J. Tankard, R. Suárez, and H. J. Welsink, eds., Petroleum Basins of South America: AAPG Memoir 62 p. 727–740.

Hantschel, T., and A. Kauerauf, 2009, Fundamentals of Basin and Petroleum Systems Modeling: Berlin, Springer-Verlag, 476 p.

Hantschel, T., B. Wygrala, M. Fuecker, and A. Neber, 2012. Modeling basin-scale geomechanics through geologic time (abs.): International Petroleum Technology Conference, Bangkok.

Hedberg, J. D., 1950, Geology of the eastern Venezuela basin (Anzoategui-Monagas-Sucre-eastern Guarico portion): Geological Society of America Bulletin, v. 61, p. 1173–1216, doi: 10.1130/0016-7606(1950)61[1173:GOTEVB]2.0.CO;2.

James, K. H., 1990, The Venezuelan hydrocarbon habitat, *in* J. Brooks, ed., Classic petroleum provinces: The Geologic Society (London), Special Publication v. 50, p. 9–35.

James, K. H., 2000a, The Venezuelan hydrocarbon habitat, part 1: Tectonics, structure, paleogeography and source rocks: Journal of Petroleum Geology, v. 23, no. 1, p. 5–53, doi: 10.1111/jpg.2000.23.issue-1.

James, K. H., 2000b, The Venezuelan hydrocarbon habitat, part 2: Hydrocarbon occurrences and generated accumulated volumes: Journal of Petroleum Geology, v. 23, no. 2, p. 133–164.

Krause, H., and K. H. James, 1989, Hydrocarbon resources of Venezuela. Their source rock and structural habitat, *in* G. E. Ericksen, M. T. Canas-Pinochet, and J. A. Reinemund, eds., Geology of the Andes and its relation to hydrocarbon and mineral resources: Circum-Pacific Council for Energy and Mineral Resources, Earth Sciences Series, v. 11, p. 405–414.

Kukla, P. A., S. C. Edwards, and K. K. Reimann, 2000, 3D petroleum systems modelling: Bridging the gap between basin and reservoir scale modelling-examples from offshore Western Australia, Extended Abstract 4258, AAPG International Conference, October 15–18, 2000, Bali, accessed May 14, 2014, www.searchanddiscovery.com/abstracts/html/2000/intl/abstracts/219.

Locke, B. D., and J. I. Garver, 2005, Thermal evolution of the eastern Serrania del Interior foreland fold and thrust belt, northeastern Venezuela, based on apatite fission track analysis, *in* H. G. AvéLallemant and V. Baker Sisson, eds., Caribbean–South American plate interactions, Venezuela: The Geologic Society of America Special Paper, v. 394, p. 315–328.

Maerten, L., and F. Maerten, 2006, Chronologic modeling of faulted and fractured reservoirs using geomechanically based restoration: Technique and industry applications: AAPG Bulletin, v. 90, no. 8, p. 1201–1226, doi: 10.1306/02240605116.

Magoon, L. B., and W. G. Dow, 1994, The petroleum system, *in* L. B. Magoon and W. G. Dow, eds., The petroleum system—from source to trap: AAPG Memoir 60, p. 3–24.

Parnaud, F., Y. Gou, J. -C. Pascual, I. Truskowski, O. Gallango, H. Passalacqua, and F. Roure, 1995, Petroleum geology of the central part of the Eastern Venezuela basin, *in* A. J. Tankard, R. Suárez-Soruco, and H. J. Welsink, eds., Petroleum basins of South America: AAPG Memoir 62, p. 741–756.

Parra, M., G. J. Sanchez, L. Montilla, O. J. Guzman, J. Namson, and M. I. Jacome, 2011, The Monagas fold-thrust belt of eastern Venezuela: Marine and Petroleum Geology, v. 28, no. 1, p. 70–80, doi: 10.1016/j.marpetgeo.2010.01.001.

Passalacqua, H., F. Fernandez, Y. Gou, and F. Roure, 1995, Deep architecture and strain partitioning in the eastern Venezuelan Ranges, *in* A. J. Tankard, R. Suárez-Soruco, and H. J. Welsink, eds., South American basins: AAPG Memoir 62, p. 667–679.

Pepper, A. S., and P. J. Corvi, 1995, Simple kinetic models of petroleum formation. Part I: oil and gas from Kerogen: Marine and Petroleum Geology Geological Society, v. 12, no. 3, p. 291–319, doi: 10.1016/0264-8172(95)98381-E.

Perez de Armas, J., 2005, Tectonic and thermal history of the western Serrania del Interior foreland fold and thrust belt and Guarico basin, north-central Venezuela: Implications of new apatite fission-track analysis and seismic interpretation, *in* H. G. Avé Lallemant and V. Baker Sisson, eds., Caribbean–South American Plate interactions, Venezuela: The Geological Society of America Special Paper, v. 394, p. 271–314.

Pindell, J. L., and K. D. Tabbutt, 1995, Mesozoic-Cenozoic Andean paleogeography and regional controls on hydrocarbon systems, *in* A. J. Tankard, R. Suárez-Soruco, and H. J. Welsink, eds., Petroleum basins of South America: AAPG Memoir 62, p. 101–128.

Prieto, R., and G. Valdes, 1992, El Furrial oil field: A new giant in an old basin, *in* M. T. Halbouty, ed., Giant oil and gas fields of the decade 1978–1988: AAPG Special Volumes M 54, p. 155–161.

Roure, F., N. Bordas-Lefloch, J. Toro, C. Aubourg, N. Guilhaumou, E. Hernandez, S. Lecornec-Lance, C. Rivero, P. Robion, and W. Sassi, 2003, Petroleum systems and reservoir appraisal in the sub-Andean basins (eastern Venezuela and eastern Colombian foothills), *in* C. Bartolini, R. T. Buffler, and J. Blickwede, eds., The Circum-Gulf of Mexico and the Caribbean: Hydrocarbon habitats, basin formation, and plate tectonics: AAPG Memoir 79, p. 750–775.

Roure, F., R. Swennen, F. Schneider, J. L. Faure, H. Ferket, N. Guilhaumou, K. Osadetz, P. Robion, and V. Vandeginste, 2005, Incidence and importance of tectonics and natural fluid migration on reservoir evolution in foreland fold-and-thrust belts: Oil and Gas Science and Technology-Revue de l'IFP, v. 60, no. 1, p. 67–106, doi: 10.2516/ogst:2005006.

Schneider, F., 2003, Basin modeling in complex area: Examples from eastern Venezuelan and Canadian foothills: Oil and Gas Science and Technology-Revue de l'IFP, v. 58, no. 2, p. 313–324, doi: 10.2516/ogst:2003019.

Schneider, F., M. Pagel, and E. Hernandez, 2004, Basin modeling in a complex area: Example from the Eastern Venezuelan foothills, *in* R. Swennen, F. Roure, and J. W. Granath, eds., Deformation, fluid flow, and reservoir appraisal in foreland fold and thrust belts: AAPG Hedberg Series, no. 1, p. 357–369.

Summa, L. L., E. D. Goodman, M. Richardson, I. O. Norton, and A. R. Green, 2003, Hydrocarbon systems of Northeastern Venezuela: Plate through molecular scale-analysis of the genesis and evolution of the Eastern Venezuela Basin: Marine and Petroleum Geology, v. 20, nos. 3–4, p. 323–349, doi: 10.1016/S0264-8172(03)00040-0.

Sweeney, J. J., and A. K. Burnham, 1990, Evaluation of a simple model of vitrinite reflectance based on chemical kinetics: AAPG Bulletin, v. 74, no. 10, p. 1559–1570.

Talukdar, S., O. Gallango, and A. Ruggiero, 1988, Generation and migration of oil in the Maturin subbasin, eastern Venezuelan basin, *in* L. Matavelli and L. Novelli, eds., Advances in organic geochemistry: Organic Geochemistry, v. 13, p. 537–547.

Terzaghi, K., 1923, Die Berechnung der Durchlässigkeitsziffer des Tones im Verlauf der hydrodynamischen Spannungserscheinungen: Sitzungsber. AkademieWissenschaft Wien, Math-naturwissenschaft KlasseIIa, Nr. 132, p. 125–138 (in German).

Wilkinson, D., 1984, Percolation model of immiscible displacement in the presence of buoyancy forces: Physical Review A, v. 30, no. 1, p. 520–531, doi: 10.1103/PhysRevA.30.520.

Wygrala, B. P., 1989, Integrated study of an oil field in the southern Po basin, northern Italy: Forschungszentrum Jülich Reports, p. 2313.

Young, G. A., 1978, Potential resources in the eastern Venezuela Basin: Boletin Informativo, AsociacionVenezolano de Geologia, Mineria y Petroleo, v. 20, p. 1–38.